Inverted vs Standard PTB7:PC70BM Organic Photovoltaic Devices. The benefit of highly selective and extracting contacts in device performance

*Ikerne Etxebarria[a,b], Antonio Guerrero[c], Josep Albero[d], Germà Garcia-Belmonte[c], Emilio Palomares[d,e] and Roberto Pacios[a,b]**

[a, *] IK4-IKERLAN, Goiru Kalea, 20500 Arrasate. Spain. E-20500. E-mail: Corresponding author: rpacios@ikerlan.es

[b] CIC microGUNE, 20500 Arrasate. Spain. E-20009.

[c] Photovoltaic and Optoelectronic Devices Group, Departament de Física, Universitat Jaume I. ES-12071 Castelló, Spain

[d] Institute of Chemical Research of Catalonia (ICIQ). Avda. Països Catalans 16. Tarragona. E-43007. Spain.

[e] ICREA. Passeig Lluís Companys, 23. Barcelona E-08010. Spain

Keywords: Inverted Organic Solar Devices, Selective Contacts, Resistive and Capacitance Losses

In this work we compare the photovoltaic performance of different cell designs, standard and inverted, for one of the most promising systems to achieve power conversion efficiencies over 10% in polymer:fullerene single cells, namely PTB7:PC70BM. Impedance Spectroscopy, Charge Extraction and Transient Photovoltage are used in order to assign the electrical losses initially observed in the current density-voltage curve and understand the main limitation of every design. While inverted devices show optimized performance in terms of bulk morphology for charge generation, transport of carriers and also for charge collection at electrodes, standard devices present additional resistive losses that are assigned to charge transfer issues at the active layer/anode interface. This additional resistance increase the overall series resistance of devices, lowers the fill factor and it is the ultimate responsible for the observed reduced device performance of standard cells in comparison to inverted ones. In this way, devices over 7.2% are reported with ZnO and MoO_3 as interlayer electrodes that act both as improved highly selective and extracting contacts in comparison to standard PEDOT:PSS and Ca/Ag. This system is electrically optimized and any performance enhancement for this particular commercial batch of polymer can only arise from optical improvements. Lower molecular weights and/or any residual catalyst impurities with respect to other batches are the only limitation to reach record efficiencies as those shown in recent works.

Published *Organic Electronics* 2014, ***15***, 2756-2762

1. Introduction

The chemical design of novel donors for polymer based organic solar cell has been, without a shadow of a doubt, the step change in the process towards achieving sufficiently high and appealing power conversion efficiencies (PCE) as to convert organic materials in a real alternative to compete in the photovoltaic market. Materials that combine low bandgap light absorption, adequate energy level positions and reasonable high carrier mobilities are considered to be the Holy Grail to move this technology one step further towards commercialization. A very recent example of active material development is a benzodithiophene derivative known as PTB7 from which devices up to 9.2% efficient are successfully processed [1]. However, this is also a good example to illustrate that improving the efficiency of a solar cell is not only a matter of the active material. Non-photoactive layers such as electrode interlayers and/or optical spacers also play a crucial role in the overall efficiency. In this way, initially reported 7.4% [2] efficient PTB7 based devices yielded 8.37% [3] and 8.1% [4], when either a polyfluorene derivative –PFN- or bathocuproine (BCP) was respectively used as cathode interlayer. Last but not least, alternative cell designs can also contribute to further enhance the light to electricity conversion [5,6]. In this regard, inverted device structures can take advantage of the vertical phase separation and concentration gradient in the active layer and offer superior contact selectivity with the potential to show surprisingly large fill factors (FF) and better long-term ambient stability [7]. This was the approach used by Z. He et al to report a drastic boost in PCE of PTB7 based devices and take it to 9.2% [1]. It is, however, important to note that all the efficiencies mentioned above are record efficiencies achieved with not always commercially available small batches of active material obtained under a very precise control of the synthesis route and conditions, especially in terms of molecular weight and impurities. When the synthesis is scaled up, those efficiencies are difficult to reproduce at different labs and average values are considerably lower.

More insight on all the internal mechanisms involved in the photovoltaic conversion of standard and inverted cells is therefore needed in order to first understand these batch to batch variations and second to clearly assign the benefits of inverted structures to concrete facts. There are several techniques that can provide valuable information on electrical parameters in operating devices. Charge Extraction (CE) informs on the charge distribution within the bulk at different applied bias and the number of charges that the system is capable of accumulating and extracting. Additionally, transient photovoltage (TPV) experiments provide information on the carrier recombination dynamics and carrier lifetime dependency on voltage [8-9]. In addition to photo-induced charge transfer measurements, impedance spectroscopy (IS) is useful to study all resistive and capacitive processes taking place in operating device such as recombination, transport mechanisms, and charge accumulation [10].

In a previous study [11], we demonstrate that transport of carriers and contact selectivity are both limiting factors for the PTB7:fullerene system. We proved that the overall device efficiency is a balance between the recombination kinetics in the bulk of the active layer, undesired resistance to transport of carriers and leakage current due to low selectivity of the contacts. We also gave

recommendations on how to solve these issues: higher proportions of fullerene can be used to reach selective contacts, and the use of additives improves charge generation and extraction and removes any issue related to transport of carriers.

In this paper, we have followed these recommendations to improve the contact selectivity and hence to routinely fabricate devices with different commercially available batches of PTB7 over 7.2%. We analyze their response in either standard or inverted configuration using all techniques aforementioned in order to identify their limitations. IS results reveal that both contact selectivity and morphology of inverted devices are fully optimized and no issues related to either transport of carriers in the active layer or charge extraction at the electrodes are observed. Any efficiency enhancement for this system has therefore to arise from optical improvements. Standard configurations show however an additional resistance that can be assigned to charge transfer issues from the active layer to the anode. This lack of an efficient extracting electric contact is the responsible for the reduced device performance.

2. Photovoltaic Characterization (JV and EQE): Identifying losses

The current density-voltage (J-V) curves for devices fabricated with the configuration ITO/PEDOT:PSS/Active layer/Ca/Ag (standard) and ITO/ZnO/Active layer/MoO3/Ag are shown in **Figure 1** along with the External Quantum Efficiency (EQE) and the absorption. The figure of merits for both devices is also listed in **Table 1**.

The EQE follows the absorption in the visible part of the spectrum, while they show an anti-symbatic behavior in the UV. This indicates that photons in the UV hardly contribute to the measured J_{SC}. EQE over 70% implies that the device development is such that the internal quantum efficiency (IQE) is already over 90%, as previously measured [2]. This practically means that all that is absorbed is efficiently converted into current. Furthermore, the light absorption of the inverted film in the UV part is considerably higher than that for the standard device, most likely due to the absorption of the ZnO film, while they absorb approximately the same within the visible part. This evidences the capability of inverted devices to provide a better control of photon harvesting from the Sun´s spectrum. The EQE is in good agreement with the J_{sc} obtained from the J-V curves for both devices. The integration over the spectrum of the EQE and the incident photon flux under AM1.5 solar irradiance is calculated to be 14.93 and 15.54 $mAcm^{-2}$ for standard and inverted devices, respectively.

The inverted device shows a better efficiency at 1 Sun primarily due to the larger photocurrent and improved FF. The larger photocurrent might be a direct consequence of the better absorbance, although morphology issues cannot be still ruled out. The enhanced FF can be in principle assigned to a lower series resistance, but the origin of this increased R_{series} for the standard device cannot be ascertained only from this set of data. Furthermore, the leakage current at -1 V is two orders of magnitude higher for the inverted devices. This excludes selectivity of the contact as the main responsible for the different performance observed, as otherwise, inverted devices should show lower PCE than standard configurations. Further experiments are thus necessary in order to shed light on all

these issues. IS under dark and under illumination, CE and TPV were carried out with the objective of clarifying where losses arise from in standard cells in comparison to inverted ones.

3. Assignment of losses

3.1 Capacitance-Voltage measurements in the dark: Selectivity of contacts and leakage current

The proportion of the cathode that is covered by fullerene can be measured in completed devices by using Capacitance-Voltage (C-V) measurements in the dark [12]. These calculations gave nearly full coverage of 93% for inverted devices and a reasonably good coverage for the standard devices of 80% (**Figure S1**). Both values are expected to be in agreement with a highly selective contact. However, these results imply that there is indeed a change in the bulk morphology when the polarity of the device is inverted. In standard devices, there is a gradient that increases the fullerene proportion towards the top electrode (Ca/Ag that acts as a cathode), while in inverted configuration most of the fullerene tends to be close to the bottom electrode (ZnO/ITO that acts now as a cathode), with a decreasing gradient of fullerene content towards the top electrode. In addition, since contact selectivity is not an issue and hence the concentration of minority carriers should be even improved for the inverted configuration, the observed results are consistent with smaller and more abundant nano domains of polymer and fullerene for the inverted device. Injected charges under dark at negative bias recombine easier giving rise to enhanced dark currents. However, this different morphology distribution does not significantly affect the device performance under illumination, as we will demonstrate later.

Different morphologies depending upon the starting substrate on top of which the same photoactive film is deposited are not unusual for polymer:fullerene solar cells since specific interactions between the organic materials and the substrate, due to mainly different surface energy and/or hydrophobicity, have been demonstrated to have a strong effect on morphology [5]. Therefore, inverted devices benefit from a more favorable vertical segregation that could additionally explain the larger leakage current at negative applied bias in dark conditions.

The origin of the increased leakage current observed for the inverted device may then also be related to either the active layer/anode interface which is not accessible for CV measurements or to a faster recombination dynamics, or a combination of both. In any case, even though the assignment cannot be made yet, it is clear that neither the leakage current nor the selectivity of the contacts is the responsible for the reduced device performance. In the following section, this issue will be clarified by studying the device response under illumination.

3.2 Impedance Spectroscopy under 1 Sun: Resistive and Capacitive processes

Impedance spectroscopy under illumination for inverted devices show mainly one arc in the Nyquist plot (**Figure 2** Up). However, at high voltages, the standard device shows another arc composed of a small additional resistance and a capacitance. The presence of this additional arc is best observed in the capacitance-frequency spectra (Figure 2 Down). The inverted device shows only one plateau in the range of frequencies between 100-1x10^5 Hz, indicating that only one capacitance dominates the device. On the contrary, the standard configuration device shows two capacitances in the form of two plateaus.

Impedance spectra can be fitted to two different equivalent circuits depending on the cell design (**Figure S2**). The inverted configuration can be modeled by a simple circuit with a recombination resistance (R_{rec}) and the chemical capacitance (C_μ) along with the series resistance due to contact and wires (R_s). The standard configuration needs an additional RC subcircuit connected in series with a resistance, R_{hf}, and a capacitance C_{hf} in parallel.

Regarding resistive processes and electrical losses in the bulk material, the low frequency response at high applied bias is connected to the recombination kinetics of the system. Alternatively, in the low applied bias region, the IS response is likely dominated by the shunt resistance. Furthermore, the high frequency response has been previously ascribed to issues related to transport of carriers in the bulk of the active layer, although it can also be related to external interfaces for morphologically optimized devices with considerably large EQE and very thin active films for which transport properties do not limit the performance of the cell. In any case, it possesses a total current loss for the device performance [13].

With respect to charge storage and carrier extraction, the device capacitance observed at low frequencies of the IS spectra for systems not severely affected by transport losses, is governed by the chemical capacitance due to excess carriers, C_μ [14-15]. This is related to the change in the occupancy by electrons of the fullerene LUMO. At low applied bias the capacitive response is dominated by the dielectric properties of the active layer. As we increase the applied bias, the density-of-states (DOS) of the acceptor LUMO levels starts being filled by electrons, and charge is stored with the consequent increase in C_μ.

3.3 Fitting results for IS at 1 Sun: Additional resistive losses limit device performance

Figure 3 shows the fitting results. Interestingly, C_μ observed for standard and inverted devices perfectly overlap (Figure 3 Up Left). An exponential increase over nearly two orders of magnitude is expected at forward bias as the DOS occupancy takes places. Furthermore, recombination resistances are very similar for both devices. The shunt resistance for the standard device is slightly higher, fully consistent with the lower leakage current observed in dark conditions, and pointing out towards morphology differences within the bulk of the active area as previously discussed.

Finally, the additional resistance observed for high frequencies for the standard configuration is rather small (below 10 Ω). However, since this is the only distinctive issue, it might well be the responsible for the reduced device performance. The origin of this additional resistance can only be related to either i) limited transport properties through the PEDOT:PSS layer or ii) charge transfer issues between the active layer and the anode that can lead to an increased overall series resistance.

3.4 Origin of additional resistive losses: Interlayer conductivity or interface issue

In order to discern which of those is more relevant, identical standard devices were made with PEDOT:PSS layers of different conductivities, ranging from the high resistivity of the Al4083 dispersion (500-5000 Ω cm) to the highly conductive PH500 (300 S cm^{-1}). All devices showed very similar PCE and FF (**Figure S3**). Furthermore, the additional arc composed of a small resistance and the capacitance is also present for all these devices in the IS spectra (not shown). Thus, we can definitely rule out the conductivity of the interlayer as the origin for this additional resistance.
This additional resistance at high frequencies can be related to the external interfaces for morphologically optimized devices with very thin active films for which transport properties do not limit the performance of the cell, as a consequence obtained EQEs are high at short circuit conditions. In any case, this additional resistance at the active film/anode interface needs to be included into the overall series resistance and added to the one referring to contacts and wires (calculated from the intercept of the high frequency arc with the x-asis and the zero value in the Nyquist plot, **Figure S4**). It, therefore, explains the larger R_{series} measured by IS for the standard cell in comparison to the inverted one (Figure S4).

3.5 Transient Photovoltage measurements: Bulk recombination processes

Two techniques are most widely used to understand recombination kinetics in working OPVs, TPV and IS. Recombination processes studied by IS under constant illumination gave very similar recombination resistance for inverted and standard cells. In TPV, the device is held at open circuit conditions. It is important to realize that at V_{oc} conditions, the net current flowing through the device is zero and the effect of the series resistance is null. IS under constant illumination, in contrast, does not operate at open circuit conditions, thus the effect of the series resistance will indeed be taken into account. This basically means that the recombination processes studied by the two techniques can be substantially different. Furthermore, the time window for monitoring the transients in TPV is restricted to the resolution of the detection system (in our system limited to μs). Although this is normally sufficiently fast to study in detail non-geminate recombination in working OPVs, which define to a large extend, the current density curve under illumination, it excludes faster recombination processes as geminate and/or surface recombination.

Figure 4 Left shows the charge density as a function of the applied light bias for standard and inverted devices measured by CE in the region from 550 to 750 mV. The density of charges for this region refers to the excess of charges that accumulate within the bulk of the device. The lineal part below 0.55 V is not of interest since it is dominated by the dielectric properties of the active layer. The fact that the density of charges grows exponentially with the applied bias suggests that there is a splitting of the quasi-Fermi levels after this threshold for both devices. In addition, it is within the same order of magnitude for both devices, with a slightly larger density of charges accumulated in the bulk of inverted devices. The recombination dynamics for a small perturbation at 470 nm for both devices measured by TPV and correlated with the density of charges obtained from CE are shown in Fig. 4 Right. As it can be observed, recombination times for charge densities under 1 Sun (4e16 e^-/cm^3) are close to 1 μs. Both are within the same order of magnitude with small differences most likely due to experimental errors rather than to different recombination mechanisms taking place in the bulk of the device. More importantly, the power law, λ, that relates the charge density with the small perturbation charge carrier lifetime [16] (i.e. the slope in Figure 4 right) gives very similar values for standard and inverted devices of 1.68 and 1.93 respectively. These very similar empirical reaction orders must imply also very similar bimolecular recombination processes under 1 Sun illumination, mainly governed by non-geminate bulk recombination, and excluding thus any geminate recombination. These similar kinetics are also in agreement with the RC constants measured by IS under illumination at 0.7 V, namely 2.3 and 1.8 μs for inverted and standard devices, respectively.

3.6 Summary: Final assignment of extra resistive losses for standard devices

In summary, we have used IS, CE and TPV to analyze in detail all the working mechanisms taking place in standard and inverted PTB7:PC70BM devices immediately after light excitation. Thanks to this detailed study we are able to identify the main limitations in device performance. Inverted devices with ZnO and MoO3 as bottom and top contact respectively present fully optimized conditions in terms of contact selectivity, bulk morphology and charge extraction at the electrodes. Standard devices with PEDOT:PSS and Ca/Ag as an anode and cathode respectively, show an additional resistance at the PEDOT:PSS/active layer that increases the overall series resistance and negatively affects the FF, and hence the PCE.

The morphology of both devices is also different. Smaller and more abundant domains of polymer and fullerene for the inverted device produce larger leakage currents in the dark, and do not significantly affect the recombination processes under illumination. The latter, along with a tiny increase in the light absorption in the UV for the inverted device, and principally, as a consequence of the increase in R_{series} for the standard device, explain the slightly larger photocurrent measured for the inverted device. All in all, the inverted device is fully electrically optimized and therefore any performance improvement for this particular commercial batch can only arise from optical improvements. Slower

molecular weights and/or any residual catalyst impurities with respect to other batches are the only limitation to reach record efficiencies as those shown in recent papers.

Experimental Section

Materials: The following materials were used as received PTB7 (1-material), $PC_{70}BM$ (SES Corporation), PEDOT:PSS (Al 4083, PH and PH500 from Heraus Precious Materials), chlorobenzene (Scharlau). Blends of donor:acceptor were prepared prior to device fabrication. PTB7 (10 mg) and $PC_{70}BM$ (15 mg) were initially dissolved in chlorobenzene inside a nitrogen glove-box (970 µl). This solution was left stirring overnight at 60˚C. After 24 h, 30 µl of diiodooctane (DIO) was added. The new solution was stirred 1 h at 70˚C just before deposition.

Device Preparation: Standard devices were fabricated in the configuration ITO/PEDOT:PSS/Active layer/Ca/Ag. Structured indium tin oxide (ITO) coated glass substrates were cleaned in subsequent acetone and isopropyl alcohol ultrasonic baths followed by 5 minutes of UV ozone treatment. A thin layer of PEDOT:PSS (dispersions with different conductivities -namely Al4083, PH, and PH500- were equally used) was spin coated on the substrates to smooth the ITO surface and to act as the hole selective contact. Substrates were annealed at 120˚C for 10 minutes in air. The PTB7:$PC_{70}BM$ film was spin-coated in nitrogen at 1200rpm (90 nm). Finally, the cathode was thermally evaporated (10 nm Ca and 100nm of Ag) at a base pressure of $4x10^{-6}$ mbar to define an OPV active area of 9 mm^2. Devices were encapsulated with an epoxy resin and a glass cover and were characterized outside the glove-box.

Inverted devices were fabricated in the configuration ITO/ZnO/Active layer/MoO3/Ag onto the same ITO starting substrates. A colloidal suspension of ZnO was prepared as reported by M. S. White *et al* [17]. This suspension was spin coated onto pre-cleaned ITO substrates at 4000 rpm. The resulting film was annealed at 150 ºC for 5 min. The PTB7:$PC_{70}BM$ film was spin-coated as in the previous case. Finally, 3nm of MoO_3 and 100nm of Ag were thermally evaporated in order to finish the device. Devices were encapsulated as before.

Device characterization: Current density-voltage (J-V) characterization was performed with a Keithley 2420 Source-Measure Unit under 100 mW cm-2 AM1.5G illumination. The calibration of the light intensity was carried out with a NREL certified monocrystalline silicon photodiode. Film thicknesses were measured by a Dektak 150 surface profilometer.

The charge extraction setup consist in a white light LED ring from $LUXEON_{(R)}$ Lumileds, these are focussed onto the devices that are held in open circuit equilibrium. Devices are connected to a DC power supply and a function generator TGP110. The light is switched off and the circuit is temporally closed, while charge are forced to pass through an oscilloscope TDS 2022 from $Tektronix_{(C)}$ that registers the drop in voltage between a resistance of 50 Ω.

In TPV measurements devices are connected to the 1 MΩ input terminal of an oscilloscope $Tektronix_{(C)}$ TDS2022 and the background illumination was obtained from a ring of 6 white LED's

from LUXEON$_{(R)}$ The small perturbation (2 mV) was applied through a light pulse (N_2 laser nominal wavelength, 50 ns pulses). Polaron-recombination rate was calculated for illumination intensities ranging from 0.1 sun to 1 sun.

Impedance spectra were performed with Autolab PGSTAT-30 equipped with a frequency analyzer module. A small voltage perturbation (20 mV rms) is applied at frequencies from 1 MHz to 1 Hz. Measurements were carried out under 1 sun light intensity calibrated with a monocrystalline silicon photodiode sweeping the DC voltage in the range 0 to V_{oc}. Recombination resistance, R_{rec}, and chemical capacitance, C_{μ} were directly extracted from the low-frequency region as previously reported [15].

Acknowledgements

We thank financial support from Generalitat Valenciana (Prometeo/2009/058, ACOMP/2009/056, ACOMP/2009/095, and ISIC/2012/008 Institute of Nanotechnologies for Clean Energies). EP thanks the ERC for the grant PolyDot, the ICIQ and ICREA for their financial support. The Spanish MINECO and the Catalan regional government is also acknowledged by the projects CTQ2012-18859 and 2009 SGR 207, respectively. RP and IE thank the European Community´s Seventh Framework Programme (FP72007-2013) under Grant no. 287818 of the X10D project for providing financial support.

References

[1] Z. He, C. Zhong, S. Su, M. Xu, H. Wu and Y. Cao. Enhanced power-conversion efficiency in polymer solar cells using an inverted device structure. *Nature Photonics*. 2012, 6, 591.

[2] Y. Liang, Z. Xu, J. Xia, S-T. Tsai, Y. Wu, G. Li, C. Ray, and L. Yu. For the Bright Future—Bulk Heterojunction Polymer Solar Cells with Power Conversion Efficiency of 7.4%. *Adv. Mater.* **2010**, 22, 1.

[3] Z. He, C. Zhong, X. Huang, W-Y. Wong, H. Wu, L. Chen, S. Su, and Y. Cao. Simultaneous Enhancement of Open-Circuit Voltage, Short-Circuit Current Density, and Fill Factor in Polymer Solar Cells. *Adv. Mater*. **2011**, 23, 4636.

[4] A. Martínez-Otero, X. Elias, R. Betancur, and J. Martorell. High-Performance Polymer Solar Cells Using an Optically Enhanced Architecture. *Adv. Optical Mater*. **2013**, 1, 37.

[5] M. Campoy-Quiles, T. Ferenczi, T. Agostinelli, P.G. Etchegoin, Y. Kim, T.D. Anthopoulos, P.N. Stavrinou, D.D.C. Bradley, J. Nelson. Morphology evolution via self-organisation and lateral and vertical diffusion in polymer:fullerene solar cell blends**.** *Nature Materials*. **2008**, 7, 158.

[6] L.M. Chen, Z. Hong, G. Li, Y. Yang . Recent Progress in Polymer Solar Cells: Manipulation of Polymer: Fullerene Morphology and the Formation of Efficient Inverted Polymer Solar Cells. *Adv. Mater*. **2009**, 21, 1434.

[7] J. Ajuria, I. Etxebarria, W. Cambarau, U. Munecas, R. Tena-Zaera, J.C. Jimeno, R. Pacios. Inverted ITO-free organic solar cells based on p and n semiconducting oxides. New designs for integration in tandem cells, top or bottom detecting devices, and photovoltaic windows *Energy Environ. Sci*.**2011**, 4, 453.

[8] A. Maurano, R. Hamilton, C. G. Shuttle, A. M. Ballantyne, J. Nelson, B. O'Regan, W. Zhang, I. McCulloch, H. Azimi, M. Morana, C. J. Brabec and J. R. Durrant. Recombination Dynamics as a Key Determinant of Open Circuit Voltage in Organic Bulk Heterojunction Solar Cells: A Comparison of Four Different Donor Polymers. *Adv. Mater*. **2010**, 22, 4987.

[9] A. Sánchez-Díaz, L. Burtone, M. Riede and E. Palomares. Measurements of efficiency losses in blend and bilayer-type zinc phthalocyanine/C60 high-vacuum-processed organic solar cells. *J. Phys. Chem. C* .**2012**, 116, 16384.

[10] A. Guerrero, L. F. Marchesi, P. P. Boix, J. Bisquert and G. Garcia-Belmonte. Recombination in Organic Bulk Heterojunction Solar Cells: Small Dependence of Interfacial Charge Transfer Kinetics on Fullerene Affinity. *J. Phys. Chem. Lett.* **2012**,3, 1386.

[11] A. Guerrero, N. F. Montcada, J. Ajuria, I. Etxebarria, R. Pacios, G. Garcia-Belmonte and E. Palomares. Charge carrier transport and contact selectivity limit the operation of PTB7-based organic solar cells of varying active layer thickness. *J. Mater. Chem. A*. **2013**,1, 12345.

[12] A. Guerrero, B. Dörling, T. Ripollles-Sanchis, M. Aghamohammadi, E. Barrena, M. Campoy-Quiles and G. Garcia-Belmonte. Interplay between Fullerene Surface Coverage and Contact Selectivity of Cathode Interfaces in Organic Solar Cells. *ACS Nano*. **2013**, 7, 4637.

[13] A. Guerrero, T. Ripolles-Sanchis, P. P. Boix and G. García-Belmonte. Series resistance in organic bulk-heterojunction solar devices: Modulating carrier transport with fullerene electron traps. *Org. Electron.*, **2012**, 13, 2326.

[14] J. Bisquert, D. Cahen, G. Hodes, S. Rühle and A. Zaban. Physical Chemical Principles of Photovoltaic Conversion with Nanoparticulate, Mesoporous Dye-Sensitized Solar Cells. *J. Phys. Chem. B.* **2004**,108, 8106.

[15] G. Garcia-Belmonte, P. P. Boix, J. Bisquert, M. Sessolo and H. J. Bolink. Simultaneous determination of carrier lifetime and electron density-of-states in P3HT:PCBM organic solar cells under illumination by impedance spectroscopy. *Sol. Energ. Mat. Sol. Cells*. **2010**, 94, 366.

[16] J. W. Ryan, J. M. Martin-Beloqui, J. Albero and E. Palomares. Nongeminate Recombination Dynamics–Device Voltage Relationship in Hybrid PbS Quantum Dot/C60 Solar Cells. *J. Phys. Chem. C*. **2013**, 117, 17470.

[17] M. S. White, D. C. Olson, S. E. Shaheen, N. Kopidakis and D. S. Ginley. Inverted bulk-heterojunction organic photovoltaic device using a solution-derived ZnO underlayer. *Appl. Phys. Lett.* **2006**, 89, 143517.

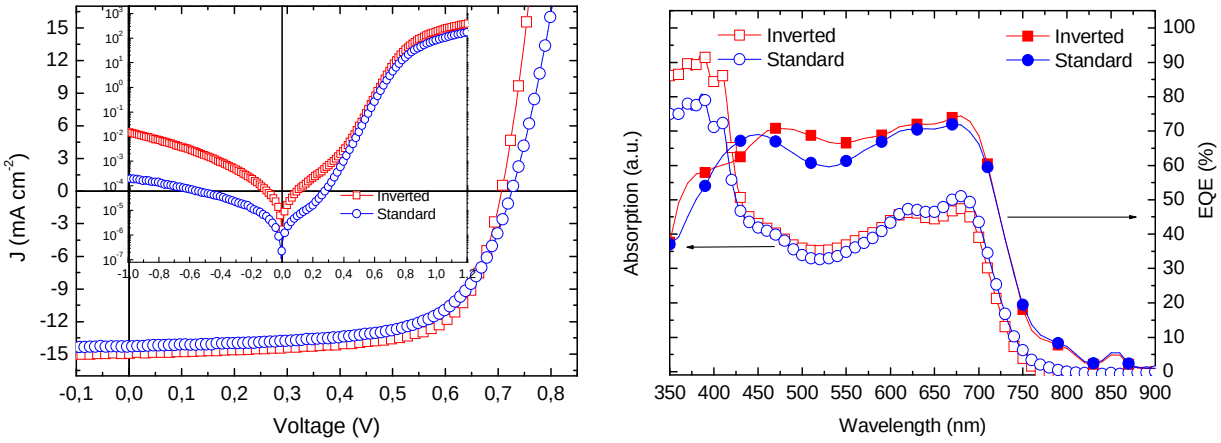

Figure 1: Left) J-V curve for the standard device design ITO/PEDOT:PSS/PTB7:PC70BM/Ca/Ag (squares) and inverted ITO/ZnO/PTB7:PC70BM/MoO3/Ag (circles). Inset: Dark J-V curves for the same devices in a log-log scale. Right) Absorption (open symbols) and External Quantum Efficiencies (filled symbols) for the same devices.

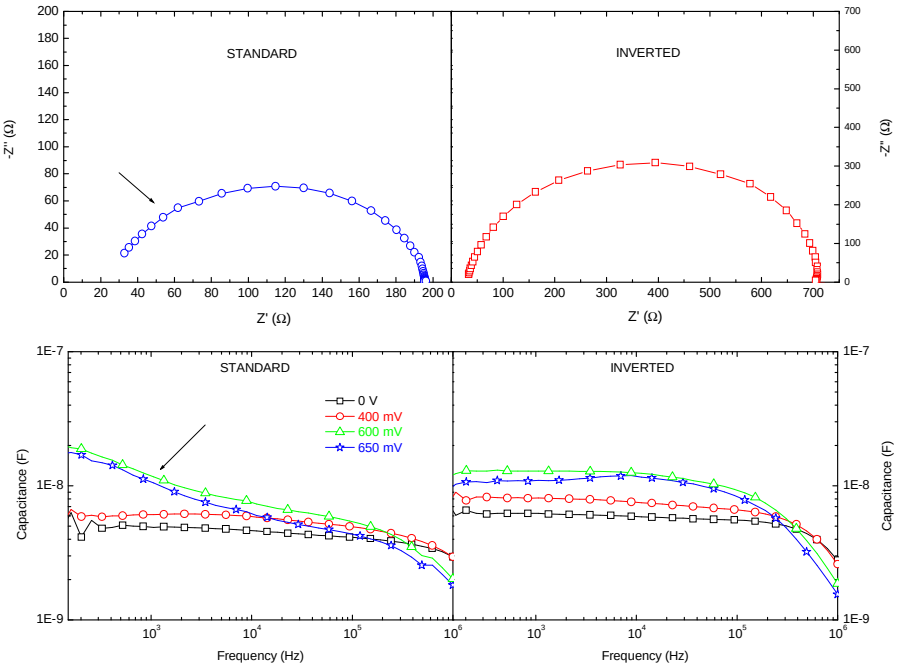

Figure 2: Up) IS response for standard (left) and inverted (right) devices measured under 1 Sun and at applied bias of 0.55 V. Down) Capacitance-Frequency spectra for standard (left) and inverted (right) devices measured under 1 Sun at selected DC applied bias. The arrow indicates the effect of the additional resistance found for standard devices.

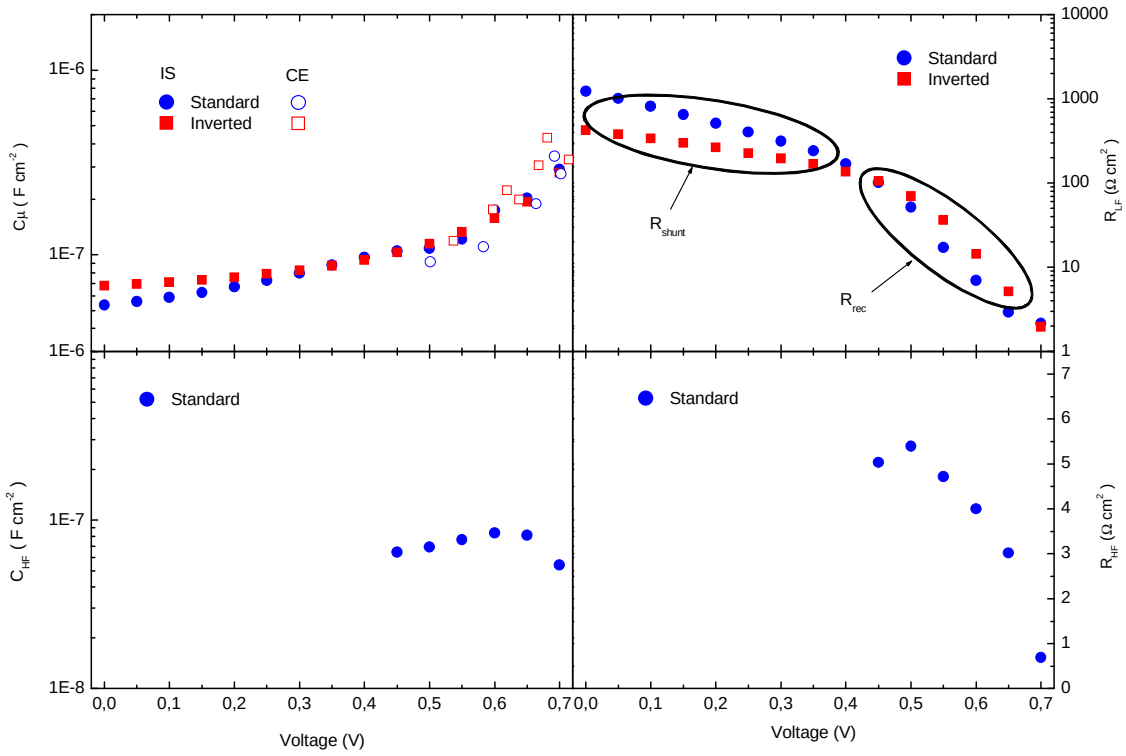

Figure 3: Fitting results, resistance (right) and capacitive (left) data, for IS measurements performed at 1 Sun light intensity for standard (circles) and inverted (squares) using the equivalent circuits given in Fig. SI2. The chemical capacitance (up left) calculated from CE measurements under equivalent conditions (open circles) is in good agreement with IS data (filled symbols)

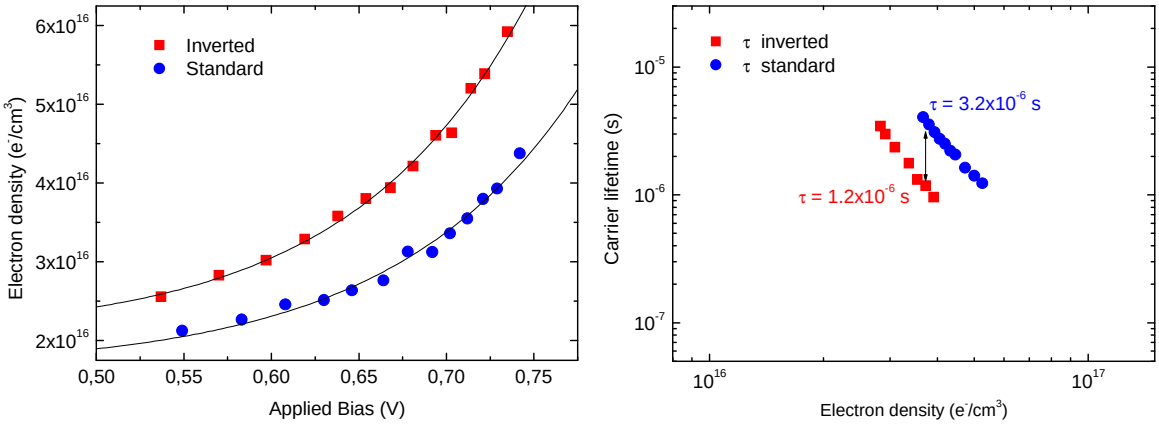

Figure 4: Left) Carrier density values as a function of the applied bias extracted from CE measurements for standard (circles) and inverted (squares) devices. The fitting of the experimental data to a first order exponential is also shown (solid lines). Right) Charge carrier lifetimes at different carrier densities.

Table 1. Figure of merits for standard and inverted devices whose J-V curves are shown in Fig. 1

Cell Design	V_{oc} [V]	J_{sc} [mAcm-2]	FF	PCE [%]
Standard	0.72	14.28	0.65	6.7
Inverted	0.70	14.93	0.69	7.2

Inverted vs Standard PTB7:PC70BM Organic Photovoltaic Devices. The benefit of highly selective and extracting contacts in device performance

*Ikerne Etxebarria[a,b], Antonio Guerrero[c], Josep Albero[d], Germà Garcia-Belmonte[c], Emilio Palomares[d,e] and Roberto Pacios[a,b]**

Supporting Information

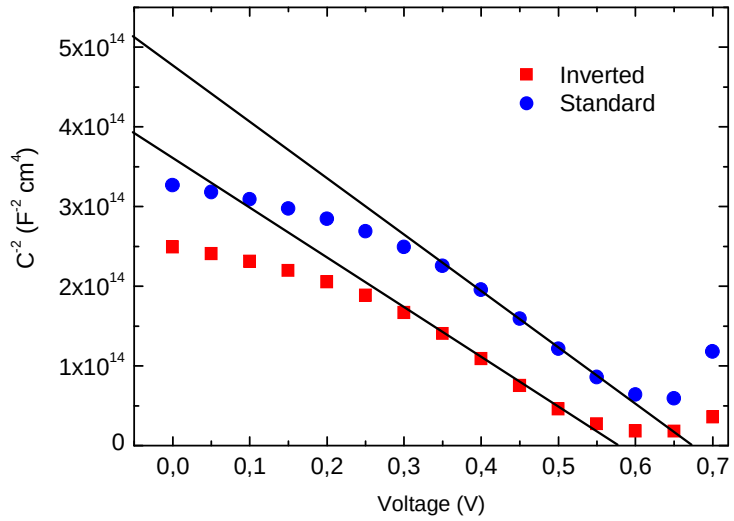

Cell Design	N [x10^{16} cm^{-3}]	V_{FB} [mV]	Cathode Fullerene Coveraged [%]
Standard	8.5	673	80
Inverted	6.6	575	93

Figure S1: Mott-Schottky analysis of devices fabricated in this work. Measurements have been carried out at a frequency of 1 kHz and dark conditions.

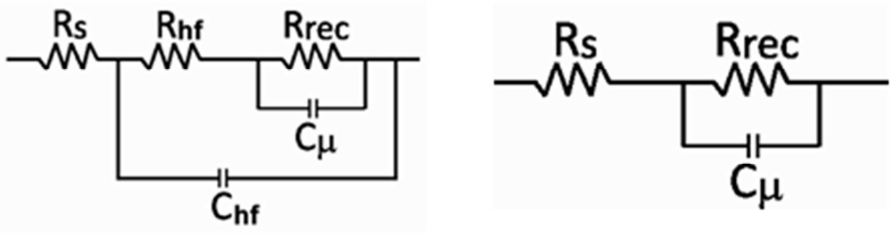

Figure S2: Equivalent circuit models used in this work for standard (left) and inverted (right) devices. R_s is the series resistance due to contacts and wires. R_{hf} and C_{hf} are the additional resistance and capacitance observed at high frequencies for standard designs. R_{rec} is the recombination resistance observed at low frequency. C_μ is chemical capacitance.

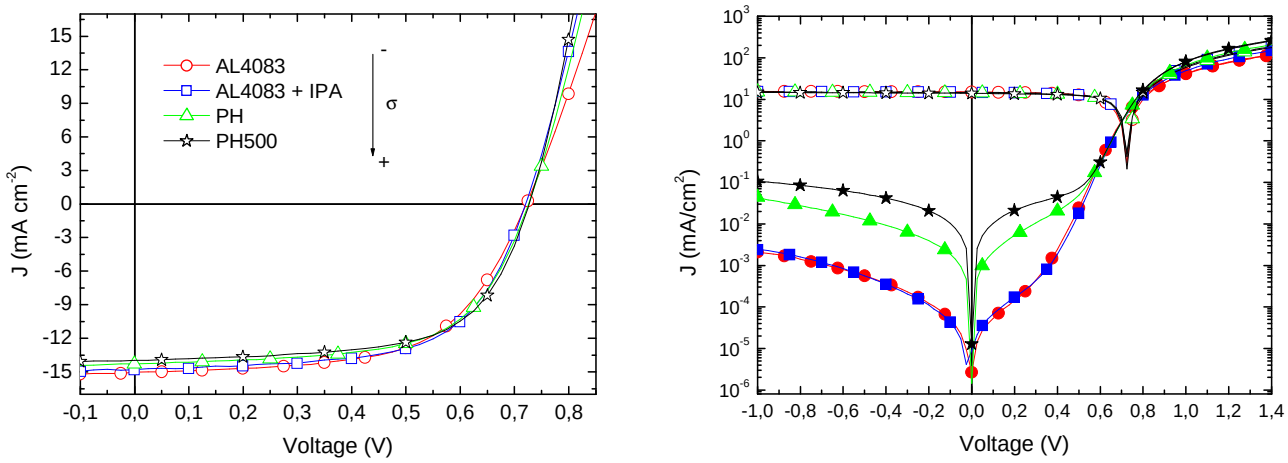

PEDOT:PSS	V_{oc} [V]	J_{sc} [mAcm-2]	FF	PCE [%]
AL4083	0.72	15.04	0.60	6.50
AL4083+IPA	0.72	14.80	0.62	6.63
PH	0.73	14.29	0.62	6.43
PH500	0.73	13.97	0.63	6.45

Figure S3: Up) J-V curves in a lin-lin scale under AM1.5G (Left) and in a log-log scale (Right) under dark (filled symbols) and under AM1.5G (open symbols) for standard devices of ITO/PEDOT:PSS/PTB7:PC70BM/Ca/Ag for different PEDOT:PSS formulations with increasing conductivities downwards. Down) Photovoltaic characterization for all the J-V curves.

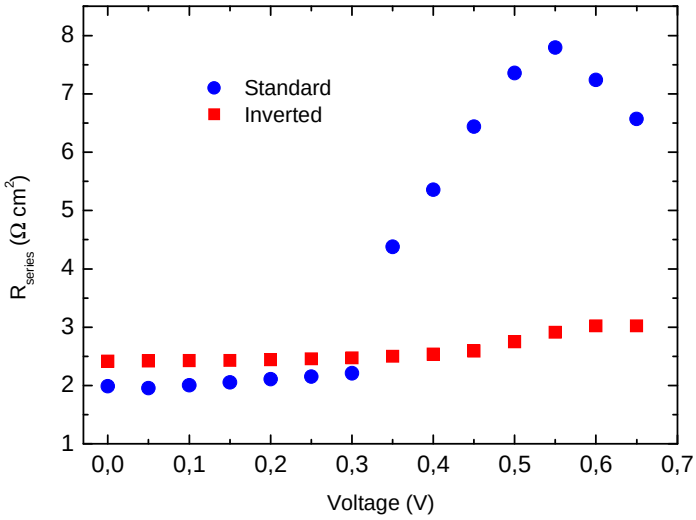

Figure S4: Calculated total series resistance using IS for standard (circles) and inverted (squares) devices. The total series resistance accounts for the contact resistance and the response at high frequencies observed only for standard devices ($R_{series} = R_s + R_{hf}$)